ELSEVIER

International Journal of Heat and Fluid Flow 22 (2001) 62–71

International Journal of HEAT AND FLUID FLOW

www.elsevier.com/locate/ijhff

An experimental investigation of two-stream mixing flow with a single delta tab

S.C.M. Yu *, P.K. Koh, L.P. Chua

Thermal and Fluids Engineering Division, School of Mechanical and Production Engineering, Nanyang Technological University, Singapore 639798, Singapore

Received 12 October 1999; accepted 18 July 2000

Abstract

A single inverted delta tab attached to the trailing edge of a splitter plate in a two-stream mixing layer has been examined experimentally using a three-component laser–Doppler anemometer. Detailed mean flow and turbulence measurements were obtained at a velocity ratio of 2:1 between the two co-flowing streams. The results showed that, when the tab was tilted to the high-speed side, streamwise vortices generated and the subsequent mixing were stronger and more intense than when tilting it to the low-speed side. Their differences in the streamwise vorticity generation mechanism were explained in relation to the tab theory proposed by Bohl and Foss (Near exit plane effects caused by primary and primary-plus-secondary tabs, AIAA Journal 37(2) (1999) 192–201). The strength of streamwise vorticity appeared to have a direct correlation with the level of turbulence generated in the cross-stream directions. Attempts were also made to quantify the effect of each (streamwise vorticity) production term in the streamwise vorticity transport equation.

1. Introduction

In several previous studies on improving jet mixing characteristics, tabs were found to be effective when they were being attached to the exit plane of a jet; see for example, the works of Samimy et al. (1993), Zaman et al. (1994), Zaman (1995) and Reader and Samimy (1996) on a circular nozzle. All these investigations have demonstrated clearly that the mass entrainment and mixing characteristics are far superior for a circular nozzle with tabs than for other nozzle geometries, including rectangular and elliptic nozzles. The mixing enhancement by the tabs can be attributed to the formation of a pair of contra-rotating vortices as the flow goes past the tab. A relatively small tab (projected surface area in the flow direction is about 3% of the total jet exit area) could generate streamwise vortices with a maximum secondary flow strength of about 20% of the main flow.

Almost all the previous investigations on tabs are primarily on their applications in jet flow. Thus, the present investigation focuses on their effects in a two-stream mixing layer. The most recent work published by Foss and Zaman (1999) focused attention on the effects of tabs in a two-stream mixing layer with laminar initial conditions. The present investigation aims to advance further the understanding on the effect of tabs in a two-stream flow situation with initial turbulent boundary layers and, incidentally, to complement the latest work of Foss and Zaman (1999) by providing detailed turbulence characteristics behind the tab.

Early research on tabs in jets by Bradbury and Khadem (1975) had speculated that the indentation on the streamwise velocity distribution around the jet axis was due to the presence of large scale traverse motions. This speculation was later confirmed by the experiments of Zaman et al. (1994), who had clearly shown that the tab produced a pair of contra-rotating streamwise vortices. The sense of rotation of the vortex pair is such that fluid from the centre of the tab base flows towards its tip and is the opposite to that found in a vortex generator (i.e., when the tip is tilted upstream).

Foss pioneered the suggestion that there are two sources for the streamwise vorticity behind the tab (see Bohl and Foss, 1999, for a summary). The first source (denoted as source 1) originates from the adverse pressure gradients formed upstream of the tab. The fluid decelerates when it comes close to the tab. A pair of contra-rotating vortices are formed as the flow attempts to go around the tab into the downstream wake. The mechanism can be described mathematically by the Navier–Stokes equation applied at the wall near the tab base.

$$\frac{1}{\rho}\frac{\partial p}{\partial z}\bigg|_{y=0} = \upsilon\frac{\partial(\Omega_x)}{\partial y}\bigg|_{y=0}. \tag{1}$$

The second source (denoted as source 2) is due largely to the vorticity shed along the sides of the tab. It should be noted that, if the approaching boundary layer upstream of the tab is thick, an additional vortex pair rotating in the opposite sense as the main pair is developed and is consistent with the horseshoe vortex system (Reader and Samimy, 1996). The

* Corresponding author. Tel.: +65-790-5595; fax: +65-791-1859.
E-mail address: mcmyu@ntu.edu.sg (S.C.M. Yu).

0142-727X/01/$ - see front matter
PII: S0142-727X(00)00072-2

Notation

Re	Reynolds number, $U_r h_{tab}/\upsilon$
h_{tab}	projected tab height at 10 mm
U_1, U_2	mean velocities of the top and bottom streams
U_r	reference mean velocity, $(U_1 + U_2)/2$
U, u'	streamwise mean and the corresponding rms velocities
V, v'	horizontal mean and the corresponding rms velocities
W, w'	vertical mean and the corresponding rms velocities
$\overline{u'v'}$, $\overline{u'w'}$, $\overline{v'w'}$	Reynolds shear stresses
U_s	secondary mean velocity, $\sqrt{V^2 + W^2}$
x, y, z	streamwise, horizontal and vertical directions
υ	kinematic viscosity
δ^*	displacement thickness (mm)
Θ	momentum thickness (mm)
H	boundary layer shape factor, δ^*/Θ
Re_Θ	Reynolds number based on the momentum thickness
Ω_x	streamwise vorticity, $=(\partial W/\partial y) - (\partial V/\partial z)$

most optimal tab shape was investigated by Zaman et al. (1994), who showed that the optimal shape of the tab should be triangular and that it must be attached firmly to the jet exit without a gap. A small gap of about half of the tab height can significantly reduce the effectiveness in streamwise vorticity generation. The maximum strength of streamwise vorticity would be generated when the tab's tip is tilted downstream at about 45° (Foss and Zaman, 1999).

As clearly shown above, with the exception of Foss and Zaman (1999), almost all the investigations concerning tabs were in free or confined jets discharging to quiescent surroundings. Hence, there is a lack of studies on the effects of tabs in a two-stream mixing layer. This certainly motivates the present investigation. The present work attempts to advance the understanding on the effect of delta tabs downstream of two flowing streams separated by a partition. The tabs considered are of triangular shape with their apex tilted downstream at ±45° relative to the main flow direction and is similar to the investigation of Foss and Zaman (1999). Table 1 shows the major parameters between the present investigation and those of Foss and Zaman (1999). The turbulence characteristics of the flow will also be examined in detail. The wind tunnel and the initial conditions are described in the next section and are followed by the instrumentation. The results are presented and discussed in Section 3, and this paper ends with a summary of the more important findings in Section 4.

2. Wind tunnel facility and instrumentation

2.1. Wind tunnel

The wind tunnel used to obtain velocity measurements in the present investigation was an open loop induction-type one with an axial fan situated on the downstream end of the test section. The upstream contraction section had an area ratio 10:1, ensuring relatively low free-stream turbulence levels on entry into the test section. A splitter plate having a thickness of 1.5 mm was installed inside the contraction section so that it was divided equally into two halves with the same area of flow. The essential features of the wind tunnel are shown schematically in Fig. 1(a). The plexi-glass test section was 200 mm high, 200 mm wide and 500 mm long. The temperature of the air inside the testing section was kept at 25°C during the course of the experiment. Different velocity ratios between the upper and lower streams were achieved by incorporating two layers of fine wire meshes on the lower half of the contraction section.

Table 1
Major experimental parameters in the present investigation and Foss and Zaman (1999)

	Foss and Zaman (1999)	Present investigation
Velocity ratio	2:1	2:1
Re_Θ (upper/lower)	932/193	219/128
Tab height	12.7 mm	10 mm
Tab base	25.4 mm	10 mm

The delta tab was cut from a single piece of sheet metal 1.5 mm thick. The entire piece was then attached immediately behind the end of the splitter plate. Scotch tape (of thickness 0.039 mm, which gives a ratio of 0.00039 relative to the upper/lower channels) was used to bridge any possible gap which may have existed at the junction. The projected tab height was used for the normalization of all the data presented here. The co-ordinate system adopted in the present investigation is shown in Fig. 1(b), in which the origin is at the center of the tab base.

2.2. Laser–Doppler anemometer

A three-component fiber-optic laser–Doppler anemometer manufactured by TSI with a 2 W argon air-cooled laser operating in the backward scattered mode was used to measure the respective velocity components. A focusing lens of 400 mm in a two-dimensional probe provided a measuring probe volume of 0.09 mm × 0.09 mm × 1.31 mm in the vertical direction (x) and 0.085 mm × 0.085 mm × 1.24 mm in the horizontal direction (y). Another one-dimensional probe provided a measuring probe volume of 0.09 mm × 0.09 mm × 1.31 mm in the lateral direction (z). The fiber-optic probes were mounted on an automated three-dimensional traversing system with an accuracy of ±0.01 mm. The six laser beams were then projected to the same point inside the test section for measurements. Bragg shifting of frequency up to 2 MHz (on each channel) was used for directional discrimination. The Doppler signals were detected by photomultipliers and processed by burst spectrum analyzers (IFA 750). Fine water particles, of sizes within the range of 5–10 μm, generated by a commercial vaporizer were used to seed the flow. Except at some regions immediately behind the trailing edge, data rates of 500–1000 Hz were normally obtainable. At each measuring point, the mean velocities, the rms of the velocity fluctuations and the Reynolds shear stresses were determined from populations of more than 5000 (on each channel) samples together with a coincidence window of 10 μs.

A careful appraisal of the errors associated with the LDA system was conducted. The sources of error mainly stemmed from velocity biasing, velocity gradient broadening (Durst et al., 1981), the accuracy of the signal processor, the finite sampling size (Yanta and Smith, 1973) and multiple seeding in

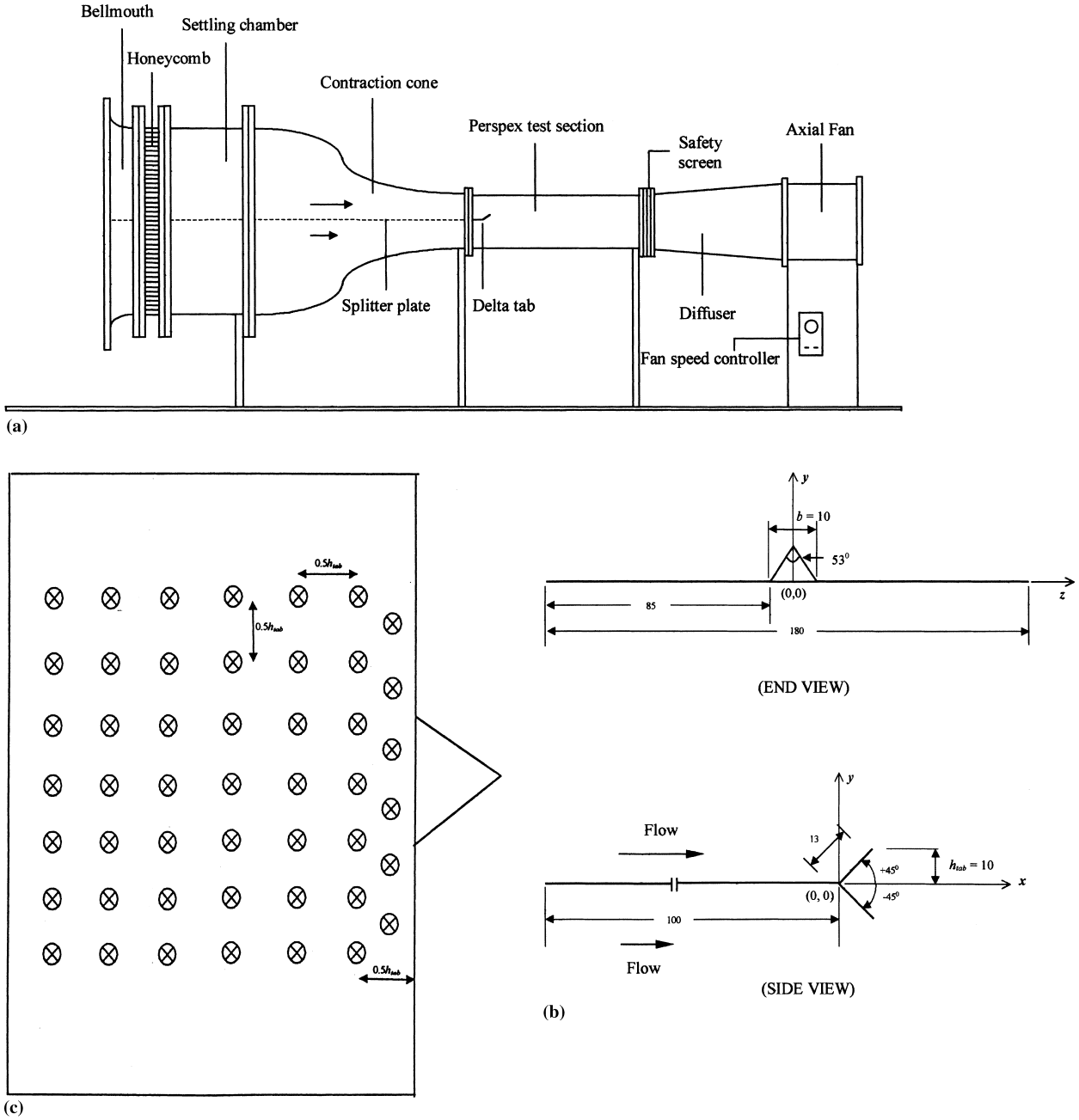

Fig. 1. Schematic of (a) the wind tunnel facilities; (b) the tab arrangement for cases 1 and 2 (all dimensions in mm); (c) pressure measurement locations.

the control volumes (Driver and Hebbar, 1987). The accuracy of the measured velocity components, U, V and W (normalized by the bulk mean velocity of the two streams, U_r), could be expected to be at about 2%, and that of the rms of the velocity fluctuations, u', v' and w' (normalized by U_r), was 5%. The Reynolds shear stresses, $\overline{u'v'}$, $\overline{u'w'}$ and $\overline{v'w'}$ (normalized by U_r^2), lay within the range of 10–20%.

2.3. Wall static pressure measurements

Wall static pressure was also measured upstream of the tab base on either side of the splitter plate. It was measured via tappings made of small stainless steel tubes (of 0.5 mm internal diameter) drilled through the splitter plate. Fig. 1(c) shows the location of the pressure measurements as well as the measurement domain upstream of the tab base. As a result of flow symmetry on either side of the tab, only the measurements in the $(-)z/h_{\mathrm{tab}}$ direction were obtained.

To minimize flow disturbances, only one point was measured at any one time. Measurements on the high-speed side were obtained first and were followed by those on the low-speed side. The differential pressure (with reference to atmospheric pressure) was obtained by connecting the output from the pressure tapping to the twin-wire resistance probe manometer designed and developed in-house by Liu (1991) via silicon tubing. The probe had a resolution of ± 0.01 mm water level so that the error of the pressure coefficient obtained (Eq. (2)) was estimated to be better than 2%.

2.4. Initial conditions

The velocity profiles on either side of the partition measured at 10 tab heights upstream of the tab base had a thickness of 9 mm (boundary layer defined at 0.99 U_{max}), see Figs. 2(a) and (b). The calculated boundary layer parameters are shown in Table 2, where δ^*, Θ, H and Re_Θ are the displacement thickness, momentum thickness, boundary layer shape factor and Reynolds number based on the momentum thickness, respectively. Both boundary layer parameters and boundary layer profiles indicated that the boundary layers on either side of the partition were turbulent. Streamwise turbulence levels outside the boundary layer region had maximum values of 1% (normalized by the mean velocity of the local stream) and rose to about 15% close to the partition.

2.5. Experimental procedures

Velocity measurements were acquired at $x/h_{tab} = 2$, 4, 6, 10 and 20 respectively. Stations close to the trailing edge had a 20×20 measurement grid (with $\Delta z = 0.1h_{tab}$ and $\Delta y = 0.1h_{tab}$), while downstream values were obtained from a 40×40 grid (with $\Delta z = 0.1h_{tab}$ and $\Delta y = 0.1h_{tab}$). Two experiments, denoted as cases 1 and 2 in the subsequent text, were conducted and are listed in Table 3.

3. Results and discussion

3.1. Mean quantities

The contours for the normalized streamwise mean velocity and the calculated streamwise vorticity at $x/h_{tab} = 2.0$ for a single tab tilted at $\pm 45°$ are shown in Figs. 3(a) and (b), respectively. When the tab is tilted to the higher-speed side, the contours are deformed into a horseshoe shape immediately behind the tab and a streamwise vortex is formed on either side of the tab axis, as may have been expected (Fig. 3(a)). For the case when the tab is tilted at $-45°$, the distribution of the contours is less distorted and the tab merely acts as an attachment surface for the higher-speed flow to penetrate into the low-speed side (Fig. 3(b)). A pair of contra-rotating vortices rotating in the same sense as that in Fig. 3(a) is also formed, but the vortex cores are located more towards the tip of the tab. There is almost a 100% difference between the strength of the peak streamwise vorticity for both cases (with the case shown in Fig. 3(a) being stronger). For the generation of the streamwise vortices in Fig. 3(a), it can be attributed to the combination of the two sources described earlier (Bohl and Foss, 1999).

For the generation of streamwise vorticity shown in Fig. 3(b), it requires some explanation. In this case, the velocity on the upper side is higher than that of the lower side, and hence, the normal vorticity shed along the tab edge from the low-speed side (i.e., source 2 mentioned above) will be generally suppressed, as shown clearly in the contour plots. Close inspection of the contours plot in Fig. 3(b) indicates that there is a small low-speed region surrounded by the higher-speed fluids around the tip (indicated by an arrow in the figure). This region becomes the source favorable to the generation of the streamwise vorticity (similar to source 2 but originating from the low-speed side). This low-velocity region is in fact formed by the retarded boundary layers when the fluid from the high-speed side follows the inclined tab surface to the low-speed side. When the boundary layers are retarded and eventually have lower momentum than the flow on the low-speed side near the region around the tip of the tab, the flow from the low-speed side then wraps around the tab edge to generate the streamwise vorticity. If we recall the net circulation results behind the delta tab (of wider base than that of the present investigation) in Fig. 8 of Foss and Zaman (1999), the strength of the streamwise vorticity increases (negatively) sharply from 0° to reach a peak at around $-45°$ to $-90°$. It can be postulated from the present experimental observation that, when the tab is tilted at angles slightly below 0°, the boundary layer on the tab surface remains attached and hence generates negligible streamwise vorticity. As the tab continues to tilt downward, the boundary layer on the tab surface grows thicker, and the momentum of the retarded boundary layer eventually becomes lower than that of the lower-speed side. This actually provides a favorable situation for the formation of streamwise vorticity (from the low-speed side to the high-speed side).

Figs. 4(a) and (b) show the pressure measurements upstream of the tab for cases shown in Figs. 3(a) and (b). The pressure coefficient,

$$C_p = [P(x,z) - P_{atm}]/(1/2\rho U_r^2), \quad (2)$$

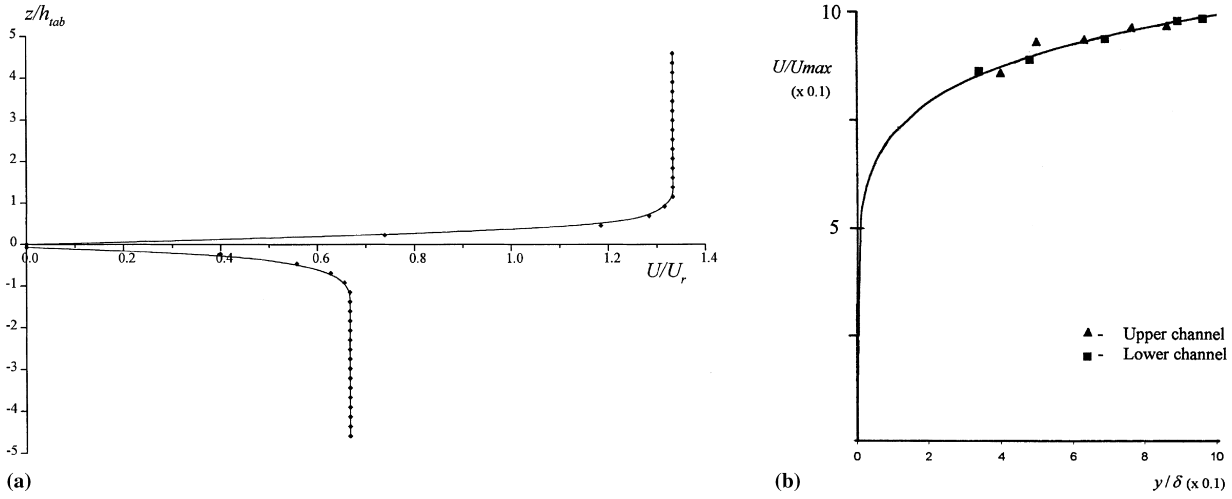

Fig. 2. (a) Profiles of the normalized streamwise mean velocities (U/U_r) at 10 h_{tab} upstream of tab base; (b) comparison of the boundary layer profiles with 1/7th power law.

Table 2
Boundary layer parameters at 10 tab heights upstream of the tab base

Stream	U (m/s)	δ^* (cm)	Θ (cm)	H	Re_Θ
Top	10.0	0.52	0.391	1.33	269
Bottom	5.0	0.48	0.34	1.41	140

Table 3
Summary of the experiments undertaken

Case	No. of tab	Velocity ratio (upper/lower)	Description
1	Single tab (+45)	2:1	High-speed flow on the side of the tab
2	Single Tab (−45)	2:1	Low-speed flow on the side of the tab

is used to characterize these values. Fig. 4(a) shows the gradual building up of the adverse pressure gradients at locations closer to the tab. The expected pressure gradients in the traverse direction (positive z) are also shown (source 1 of the streamwise vorticity formation). Comparing to the C_p distribution of Fig. 4(b) when the tab is tilted to the low-speed side, the built up of the adverse pressure gradients is not apparent even at locations very close to the tab base. Favorable pressure gradients are observed instead. This may explain why the flow remains attached to the tab surface found in Fig. 3(b). This further shows that source 1 for the streamwise vorticity formation for this case would not be the dominant source. More importantly, the comparison between these two cases highlights the fact that the generation of the streamwise vorticity by the tab is stronger when it is placed on the high-speed side. When the tab is placed on the high-speed side, both sources for the streamwise vorticity generation are operative. When the tab is placed on the low-speed side, only source 2 is operative.

3.2. Turbulence quantities

Fig. 5 shows contours of all six independent Reynolds stresses, at $x/h_{tab} = 2.0$ for case 1. The streamwise component of turbulence, u'/U_r in Fig. 5(a), is qualitatively what one would expect from flow passes over a triangular obstacle and convection of pre-existing boundary layer turbulence by the streamwise vortices from both sides of the partition. The horseshoe shape of the contour distribution follows closely that of the mean quantities in Fig. 4(a), and the region of the highest magnitude appears above the tab, which coincides with the steep velocity gradients (in both y and z directions around the tab).

Figs. 5(b) and (c) show spectacular and symmetrical maxima at regions for the fluctuations in the vertical (v'/U_r) and lateral (w'/U_r) directions near the vortex cores for case 1. It should be noticed that the maxima do not reside exactly at the same locations for both components. There is also a maximum above the tab in both cases. There is no evidence that there is large-scale lateral wandering of the streamwise vortices, which would almost certainly lead to large u'-component fluctuations in regions of large $\partial U/\partial z$, and would also smear out the peaks in v'- and w'-component fluctuations.

The contours of the normalized shear stress component $\overline{u'v'}$ shown in Fig. 5(d) are negative at the shear layer regions and at region above the tab. Within the streamwise vortices, the values are mainly positive, and their magnitude are lower than those of the negative region by almost 50%. The contours of $\overline{u'w'}$ and $\overline{v'w'}$ in Figs. 5(e) and (f) show anti-symmetrical distribution about the tab axis within the vortex region, as may have been expected. The qualitative explanation for the behavior of the three Reynolds shear stresses is that each tends to transport momentum from high-velocity to low-velocity regions, and the vortices tend to rotate fluid about the x-axis. For example, in Fig. 5(d), the negative $\overline{u'v'}$ region above the tab, generated in the region of positive $\partial U/\partial y$ regions, when rotated anti-clockwise, become the negative $\overline{u'w'}$. Similarly, the negative $\overline{u'v'}$ region above the tab, when rotated clockwise, becomes the positive $\overline{u'w'}$. The streamwise mean vorticity plot in Fig. 3(a) shows that the average is about $0.1U_r$ m^{-1} over a large part of the vortex region, implying that the rate of rotation is locally about one revolution per meter of streamwise travel. Thus, rotation through angles of the order of 90° certainly occurs at the stations further downstream.

The production terms for the normal stresses in the Reynolds stresses equations may be written as (see Bradshaw et al., 1981, p. 28)

$$G(u'^2) = -2\left(\overline{u'w'}\frac{\partial U}{\partial z} + \overline{u'v'}\frac{\partial U}{\partial y} + u'^2\frac{\partial U}{\partial x}\right), \tag{3}$$

$$G(v'^2) = -2\left(\overline{v'w'}\frac{\partial V}{\partial z} + v'^2\frac{\partial V}{\partial y} + \overline{u'v'}\frac{\partial V}{\partial x}\right), \tag{4}$$

$$G(w'^2) = -2\left(w'^2\frac{\partial W}{\partial z} + \overline{v'w'}\frac{\partial W}{\partial y} + \overline{u'w'}\frac{\partial W}{\partial x}\right). \tag{5}$$

In analyzing the production of various fluctuation components, we assume that $\partial U/\partial x$, $\partial V/\partial x$ and $\partial W/\partial x$ are small relative to the other terms. This is almost true at stations very close to the trailing edge. The signs of $\overline{u'w'}$, $\overline{u'v'}$ and those of $\partial U/\partial y$, $\partial U/\partial z$ (i.e., the first and second term in Eq. (3)) are essentially the opposite at regions of high u-component fluctuation, for example, above the tab. This implies that, as the flow goes past the tab, the increase in the gradients of the shear layer around the tip of the tab enhance the generation of turbulence. However, no such effect is found in case 2. The maximum u'-component fluctuation measured on this plane is on average 50% higher in case 1 than in case 2.

The generation of the v'-component and w'-component fluctuations provide some interesting observations. The peaks of both v'-component and w'-component distribution appear at regions within the streamwise vortices. This may not be too surprising because the first term in Eq. (4) and the second term in Eq. (5) indicate clearly that the generation of the two intensities relate directly to the components of streamwise vorticity ($\Omega_x = (\partial W/\partial y) - (\partial V/\partial z)$). The signs of $\overline{v'w'}$ are opposite to the gradients, resulting in an overall positive contribution. The observation shows clearly the effects of streamwise vorticity in turbulence generation. As a result of the peaks in the v'- and w'-component fluctuations, the diffusion terms, $\partial v'^3/\partial y$ and $\partial w'^3/\partial z$, should be decreasing slowly away from the vortex cores indicating that diffusion effects are important at the stations further downstream.

Based on the present measurements obtained on this plane, the formation of streamwise vorticity enhances the production of turbulence in the lateral and vertical directions. Although dissipation may also be concentrated at around the same region, it appears that the dissipation does not balance with the production, and hence, strong diffusion effects appears laterally and vertically. As shown by the measurements at the planes further downstream, the high v'- and w'-component fluctuations diffuse significantly from the vortex core regions to the surroundings (case 1 in particular), and at the last station

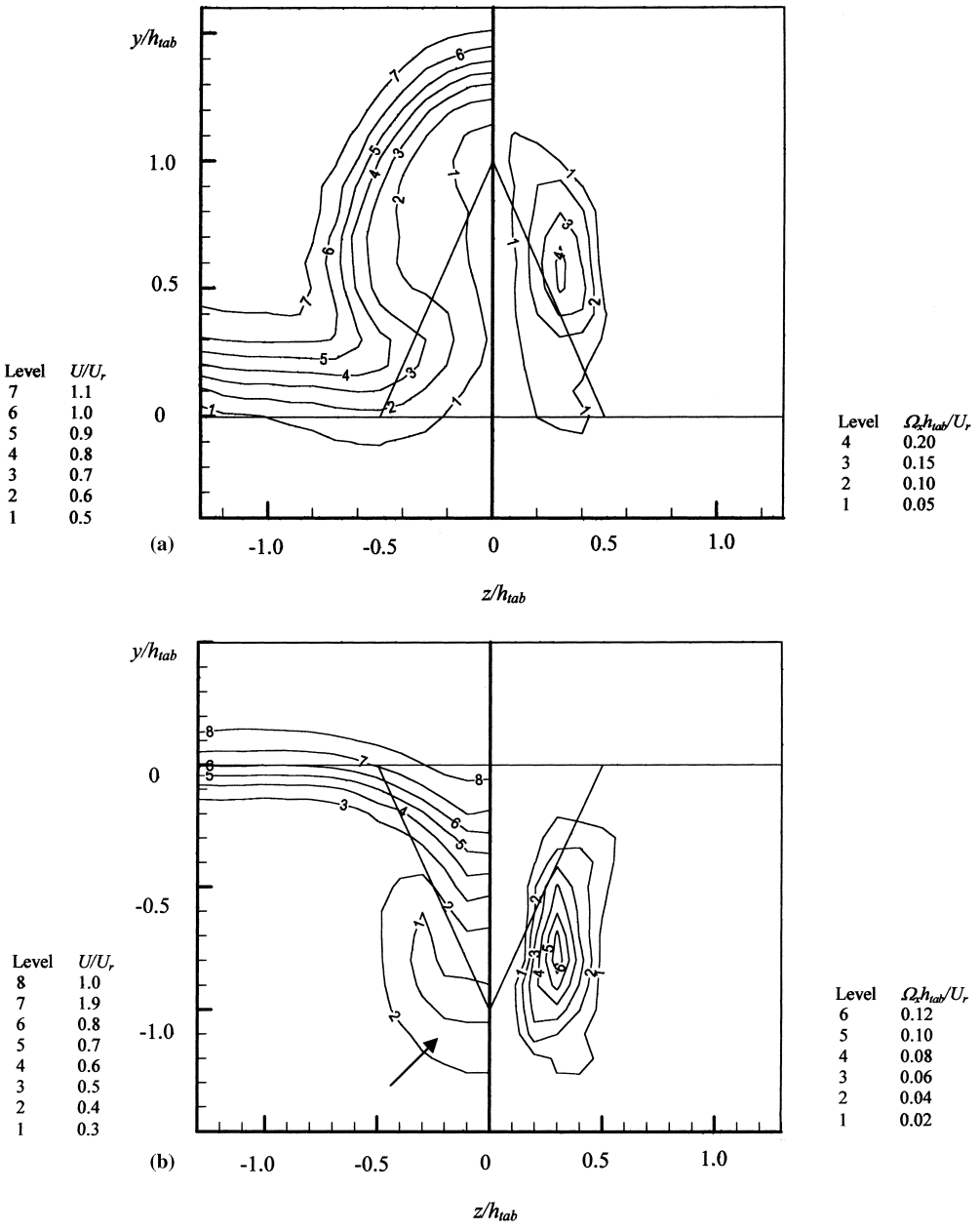

Fig. 3. Contours of normalized streamwise mean velocity (U/U_r) and streamwise vorticity $(\Omega_x h_{tab}/U_r)$ for (a) case 1 at $x/h_{tab} = 2.0$ and (b) case 2 at $x/h_{tab} = 2.0$.

measured, the level of v' and w' are almost uniform across the shear layer.

3.3. Streamwise vorticity production at the wake

The streamwise mean vorticity transport equation may be written as (Bradshaw et al., 1981, p. 229):

$$\frac{D\Omega_x}{Dt} = \underbrace{\Omega_x \frac{\partial U}{\partial x}}_{P_1} + \underbrace{\frac{\left(\Omega_y \frac{\partial U}{\partial y} + \Omega_z \frac{\partial U}{\partial z}\right)}{P_2}}_{P_2} + \underbrace{\frac{\frac{\partial}{\partial x}\left(\frac{\partial \overline{u'v'}}{\partial z} - \frac{\partial \overline{u'w'}}{\partial y}\right)}{P_3}}_{P_3} + \underbrace{\frac{\left(\frac{\partial^2}{\partial y \partial z}(v'^2 - w'^2)\right)}{P_4}}_{P_4} + \underbrace{\frac{\left(\frac{\partial^2}{\partial z^2} - \frac{\partial^2}{\partial y^2}\right)}{P_5}}_{P_5}(\overline{v'w'}) + \upsilon \nabla^2 \Omega_x. \quad (6)$$

Apart from the viscous (sixth) term, the first five terms on the right-hand side of the equations, denoted as P_1, P_2, P_3, P_4 and P_5, are essentially the production terms for the streamwise vorticity. They can be broadly divided further into two groups: P_1 and P_2 describe secondary flow production of the first kind (pressure-driven), while P_3, P_4 and P_5 are concerned with secondary flow production of the second kind (Reynolds stress-driven). The two sources of streamwise vorticity as the flow goes past the tab have been described in detail by Zaman et al. (1994) and Bohl and Foss (1999). The focus of the present discussion will therefore be on the effects of each production term on the decay (or growth) of streamwise vorticity with downstream distance. Due to space constraint, only the results in case 1 will be presented here.

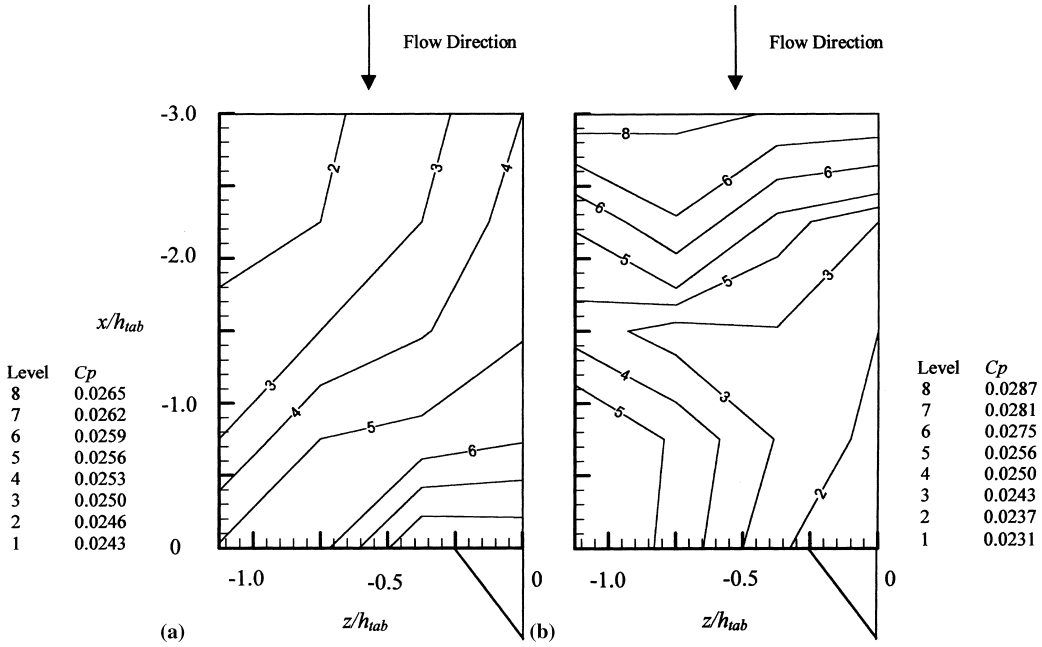

Fig. 4. Contours of upstream pressure coefficient (C_p) on the high-speed side of (a) case 1 and (b) case 2.

The first term on the right-hand side represents the vortex stretching effect (P_1) due to the streamwise mean flow acceleration. The effect of this term is difficult to quantify by examining the streamwise mean velocity distribution on a particular cross-sectional plane alone. However, qualitatively, the region which appears immediately behind the tab is initially occupied by low-momentum fluids as a result of the tab blockage effect (cf. Fig. 3(a) for case 1). As the flow progresses further downstream, this velocity defect region is rapidly filled by the higher-momentum fluids from the surroundings as a result of the streamwise vorticity generated. Hence, the U is likely to increase in the streamwise direction, and this, in turn, may provide a positive production to the streamwise vorticity at the corresponding region. It should be noted that after $x/h_{tab} = 6.0$, the flow becomes more uniformly distributed in both the y and z directions, i.e., the stretching effects should be confined to the region immediately after the tab.

The contours for P_2 in Fig. 6(a) show that they have the same sign as the streamwise vorticity on either side of the tab axis. This shows that the normal vorticity shed along the edge of the tab (when it is tilted downstream) contributes positively to the production of the streamwise vorticity on either side of the tab. This clearly shows the effects of the source 1 described earlier by Bohl and Foss (1999). Contours for P_3 are shown in Fig. 6(b). The plot shown here disregards the streamwise derivative, $\partial/\partial x$. The contour distribution is almost symmetrical with respect to the tab axis at $z = 0$. The order of magnitude in general is very low compared to that found in Fig. 6(a). It should be mentioned that, although the signs of the highest regions are in fact the opposite to those of streamwise vorticity on either side of the tab axis, their overall contribution should be considered together with the variation in the streamwise direction. Subsequent examination of the variation of this term with the downstream station at $x/h_{tab} = 4.0$ suggests that the variation in magnitude is very small but generally lower at the downstream plane. It can therefore be concluded that the contribution from this term is far less than P_2, but it is still positive.

The anisotropy of the flow appears mainly within the shear layer region, and the vertical (v') components are always higher than the lateral (w') components. The gradients in both y and z directions are always positive. This provides an overall positive production to the streamwise vorticity by P_4 (Fig. 6(c)). It should be noticed that the peaks of P_4 do not coincide exactly with the streamwise vortices, but the overall effect of this term is still an anti-clockwise sense of rotation (Perkins, 1970). Subsequent examination of the secondary flow velocity vector plots at the same region clearly shows that the direction of the flow is in agreement with the speculation above. However, it should be mentioned that the order of magnitude of this term is one order lower than that of P_2, so that its contribution to the overall strength of streamwise vorticity is very small.

The production term due the shear stress component $\overline{v'w'}$, P_5, is shown in Fig. 6(d). The distribution of the contours form a mirror image with respect to the tab axis, and the positive and negative regions appear alongside each other. The magnitude of the contour level is only lower than that of P_2 but higher than the other three. The locations of the positive and negative regions are interesting when compared to the locations of streamwise vorticity in Fig. 3(a). The positive region actually coincides with the core of the streamwise vorticity contours, and the strength of the streamwise vorticity drops gradually at the edge of the negative region. This comparison highlights the important contribution of this term to the generation of streamwise vorticity. Considering only the region on the right-hand side of the tab axis, the sign of the shear stress $\overline{v'w'}$ is mainly positive (Fig. 6(d)) within the streamwise vortex, and it reduces in magnitude away from the vortex. The shear stress gradients on the side near the tab axis are positive in both y and z directions, causing an overall positive contribution, and the opposite is true for the side away from the tab axis. It should be noticed that, since the streamwise vorticity generated is much stronger than the suppressing effect of the $\overline{v'w'}$ gradients, the direction of the net flow is still in the anti-clockwise sense.

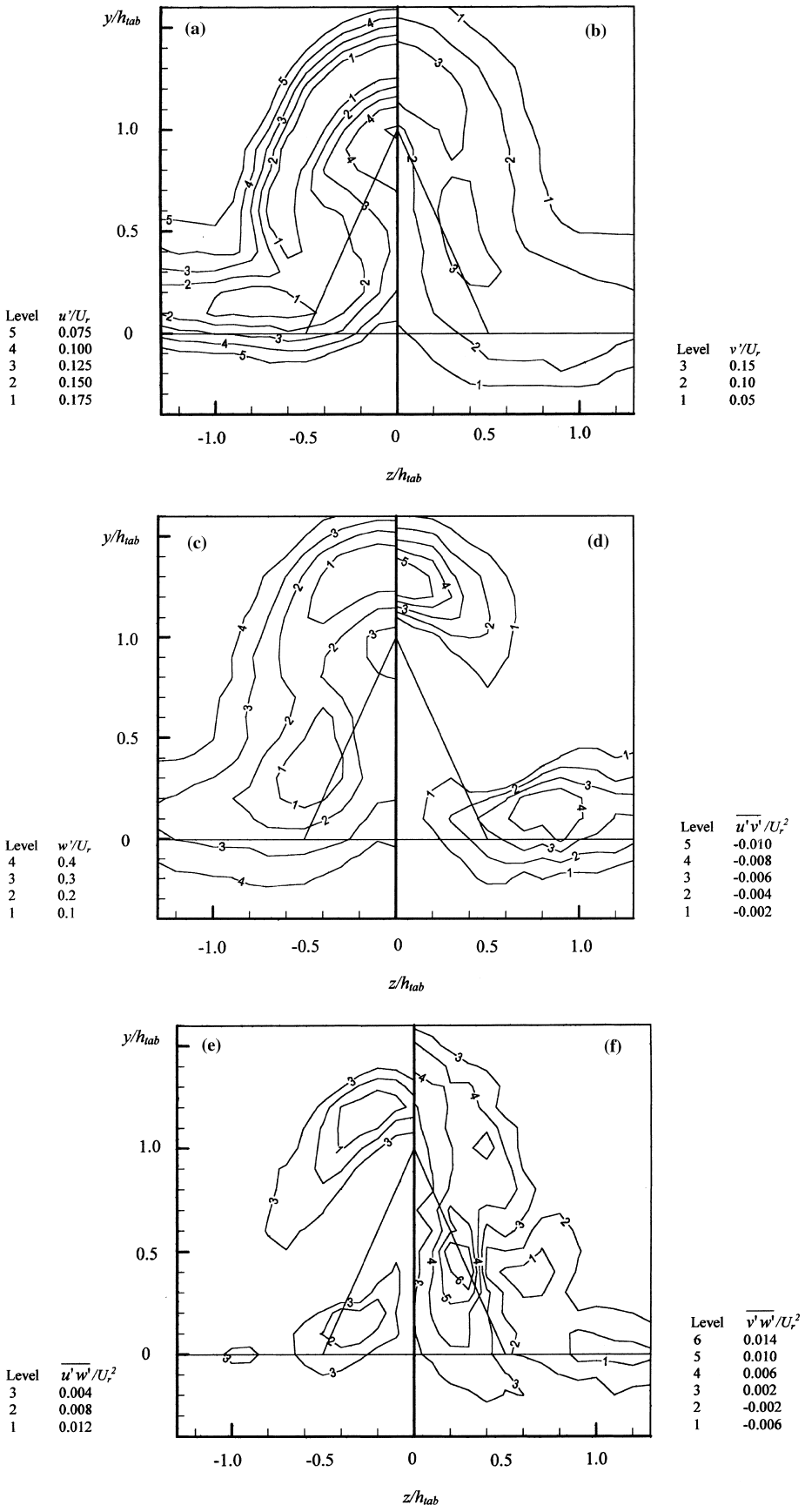

Fig. 5. Contours of the normalized (a) streamwise component of fluctuations (u'/U_r); (b) vertical component of fluctuations (v'/U_r); (c) lateral component of fluctuations (w'/U_r); and Reynolds shear stresses (d) ($\overline{u'v'}/U_r^2$); (e) ($\overline{u'w'}/U_r^2$); and (f) ($\overline{v'w'}/U_r^2$) for case 1 at $x/h_{tab} = 2.0$.

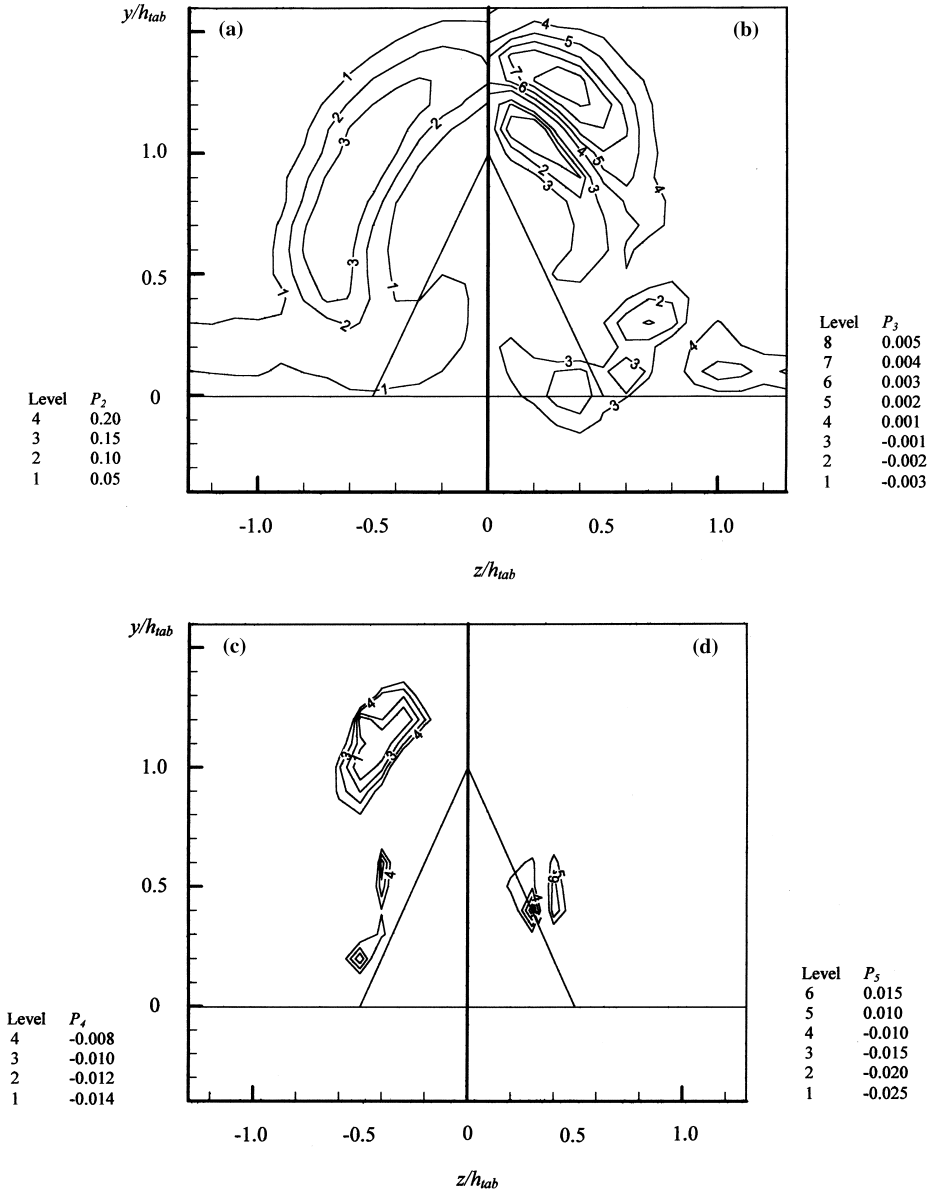

Fig. 6. Contours of streamwise vorticity production terms (a) P_2, (b) P_3, (c) P_4 and (d) P_5 for case 1 at $x/h_{\text{tab}} = 2.0$ (cf. Eq. (6)).

As discussed above, the magnitude of the production terms is generally low except for P_2. This term can be viewed as the source 2 in the tab theory of Bohl and Foss (1999). In summary, the other production terms have some localized effects on the flow field but they should not have any significant effect on the overall trend of streamwise vorticity development.

4. Summary and concluding remarks

The effects of a single inverted delta tab in a two-stream mixing flow situation have been investigated using a three-component laser–Doppler anemometer. The distortion in the streamwise mean velocity flow fields and the generation of the streamwise vorticity that resulted from the introduction of the tab have been established via measurements of three mean velocity components and six Reynolds stress components in the present investigation. The results have clearly shown that when the tab is tilted to the high-speed side, it enhances mixing between the two streams better than when tilted on the side of the low-speed flow. When the tab is placed on the high-speed side, both sources (1 and 2, as defined by Bohl and Foss, 1999) for streamwise vorticity generation are operative. When the tab is placed on the low-speed side, only source 2 is operative. Source 1 is related to the upstream adverse pressure gradients indicated by Eq. (1), while source 2 is due to the shedding of normal vorticity along the tab edge.

A high level of fluctuations in the lateral directions (v' and w') is found at regions around the vortex cores through the combined (and positive) contribution of the streamwise vorticity and Reynolds shear stress component $\overline{v'w'}$. Of particular note is that these high lateral fluctuation regions appear at a similar location as the high dissipation regions in the tab experiments conducted by Foss and Zaman (1999). This observation suggests that the production of turbulence in the lateral directions is strongly associated with streamwise vorticity and that the imbalance of production and dissipation leads to significant diffusion in the stations further downstream.

An analysis of the contribution of respective production terms in the streamwise vorticity transport equation shows that the anisotropy and Reynolds stresses generated in the flow may have some local effects on the distribution and development of streamwise vorticity. However, the dominant production term appears to be the spanwise vorticity shed along the edge of the tab, which also corresponds to source 2 mentioned above.

Acknowledgements

Financial support for this project from the Academic Research Fund, and the graduate scholarship for Mr. P. K. Koh from the School of Mechanical and Production Engineering, are gratefully acknowledged.

References

Bohl, D., Foss, J.F., 1999. Near exit plane effects caused by primary and primary-plus-secondary tabs. AIAA Journal 37 (2), 192–201.

Bradbury, L.J.S., Khadem, A.H., 1975. The distortion of a jet by tabs. Journal of Fluid Mechanics 70, 801–813.

Bradshaw, P., Cebeci, T., Whitelaw, J.H., 1981. Engineering Calculation Methods for Turbulent Flow. Academic Press, New York.

Driver, D.M., Hebbar, S.K., 1987. Experimental study of a three dimensional, shear driven turbulent boundary layer. AIAA Journal 25, 35–42.

Durst, F., Melling, A., Whitelaw, J.H., 1981. Principles and Practice of Laser–Doppler Anemometry. Academic Press, London.

Foss, J.K.F., Zaman, K.B.M.Q., 1999. Large and small scale vortical motions in a shear layer perturbed by tabs. Journal of Fluid Mechanics 382, 307–329.

Liu, C.Y., 1991. Twin-wire resistance probe manometer for very low differential pressure measurement. Transactions of the Institute of Measurement and Control 13 (4), 211–214.

Perkins, H.J., 1970. The formation of streamwise vorticity in turbulent flow. Journal of Fluid Mechanics 44, 721–740.

Reeder, M.F., Samimy, M., 1996. The evolution of a jet with vortex-generating tabs: real time visualization and quantitative measurements. Journal of Fluid Mechanics 331, 73–118.

Samimy, M., Zaman, K.B.M.Q., Reeder, M.F., 1993. Effect of tabs on the flow and noise field of an axisymmetric jet. AIAA Journal 31, 609–619.

Yanta, W.J., Smith, R.A., 1973. Measurements of turbulence transport properties with a laser–Doppler velocimeter. AIAA Paper no. 73–169.

Zaman, K.B.M.Q., 1995. Axis switching and spreading of an asymmetric jet: the role of coherent structure dynamics. Journal of Fluid Mechanics 316, 1–27.

Zaman, K.B.M.Q., Reeder, M.F., Samimy, M., 1994. Control of an axisymmetric jet using vortex generators. Physics of Fluids 6 (2), 778–793.